# Supplemental Material for "Superconducting triangular islands as a platform for manipulating Majorana zero modes"

Aidan Winblad<sup>1</sup> and Hua Chen<sup>1,2</sup>

<sup>1</sup>Department of Physics, Colorado State University, Fort Collins, CO 80523, USA <sup>2</sup>School of Advanced Materials Discovery, Colorado State University, Fort Collins, CO 80523, USA

#### I. ANALYTIC SOLUTIONS OF THE KITAEV TRIANGLE

In this section we present some analytic results related to the 3-site Kitaev triangle.

We start from the 1D Kitaev chain Hamiltonian with complex nearest-neighbor hopping  $-te^{i\phi}$  and p-wave pairing  $\Delta e^{i\theta}$  in the Kitaev limit  $(t = \Delta > 0, \mu = 0)$ :

$$H = \sum_{n} \left( -te^{i\phi} c_n^{\dagger} c_{n+1} + \Delta e^{i\theta} c_n c_{n+1} + \text{h.c.} \right)$$
 (1)

In the Majorana fermion basis  $a_n = c_n + c_n^{\dagger}$ ,  $b_n = -i(c_n - c_n^{\dagger})$  the Hamiltonian becomes

$$H = -\frac{it}{2} \sum_{n} \left[ (S_{\phi} - S_{\theta}) a_n a_{n+1} + (S_{\phi} + S_{\theta}) b_n b_{n+1} + (C_{\phi} - C_{\theta}) a_n b_{n+1} - (C_{\phi} + C_{\theta}) b_n a_{n+1} \right]$$
(2)

where  $S_{\phi} \equiv \sin \phi$ ,  $C_{\phi} \equiv \cos \phi$ , etc. Therefore, when  $\phi = \theta$ ,  $a_n$  becomes decoupled from  $a_{n+1}$  and  $b_{n+1}$ , and  $a_1$  drops out from the Hamiltonian. Similarly, when  $\phi = \theta + \pi$ ,  $b_1$  becomes isolated. To find the other MZM, we note that when  $\phi = \theta$ , terms involving  $a_N$  and  $b_N$  in the Hamiltonian are

$$H_N = -itb_{N-1}(S_\phi b_N - C_\phi a_N). \tag{3}$$

Considering the unitary transformation

$$\begin{pmatrix} a_N' \\ b_N' \end{pmatrix} \equiv \begin{pmatrix} C_{\phi} & -S_{\phi} \\ S_{\phi} & C_{\phi} \end{pmatrix} \begin{pmatrix} a_N \\ b_N \end{pmatrix} \tag{4}$$

we have

$$H_N = itb_{N-1}a_N' \tag{5}$$

Therefore the other MZM is  $b'_N = S_{\phi}a_N + C_{\phi}b_N$ . Similarly, when  $\phi = \theta + \pi$  the other MZM is  $a'_N \equiv C_{\phi}a_N - S_{\phi}b_N$ . For the 3-site Kitaev triangle at the initial configuration  $\phi_1$ , if the three edges were isolated from each other, the MZM would have been

$$1-2: a_1, b_2$$
 (6)

$$2-3: b_2, \frac{1}{2}a_3 + \frac{\sqrt{3}}{2}b_3$$

$$3-1: \quad a_1, \ \frac{\sqrt{3}}{2}a_3 + \frac{1}{2}b_3$$

One can therefore see that the two MZM at site 3 are not compatible with each other.

We next solve for the excited states of the Kitaev triangle at the initial configuration  $\phi_1$ . The Hamiltonian in the Majorana basis is

$$H = -\frac{it}{2} \left( -2b_1 a_2 - \sqrt{3}a_2 a_3 + a_2 b_3 + \sqrt{3}b_1 b_3 - b_1 a_3 \right) = \frac{1}{2} \Gamma h \Gamma^T$$
 (7)

$$\Gamma \equiv (b_1, a_2, a_3, b_3)$$

$$h \equiv -it \begin{pmatrix} 0 & -1 & -\frac{1}{2} & \frac{\sqrt{3}}{2} \\ 1 & 0 & -\frac{\sqrt{3}}{2} & \frac{1}{2} \\ \frac{1}{2} & \frac{\sqrt{3}}{2} & 0 & 0 \\ -\frac{\sqrt{3}}{2} & -\frac{1}{2} & 0 & 0 \end{pmatrix} = t \left( -\frac{1}{2}\sigma_0\tau_y - \frac{1}{2}\sigma_z\tau_y - \frac{1}{2}\sigma_y\tau_z + \frac{\sqrt{3}}{2}\sigma_x\tau_y \right)$$

h has the following symmetry:

$$O = \left(\frac{\sqrt{3}}{2}\sigma_x - \frac{1}{2}\sigma_z\right)\tau_y\tag{8}$$

We therefore rotate the Hamiltonian so that O becomes diagonal using the following unitary operator

$$U = e^{-\frac{i\pi}{3}\sigma_y} \otimes e^{i\frac{\pi}{4}\tau_x} \tag{9}$$

which leads to

$$U^{\dagger}OU = \text{Diag}(1, -1, -1, 1) \tag{10}$$

U therefore block-diagonalizes h as

$$U^{\dagger}hU = \frac{t}{2} \begin{pmatrix} 1 & & -1 \\ & -1 & 1 \\ & 1 & -3 \\ -1 & & 3 \end{pmatrix}$$
 (11)

which can then be diagonalized by

$$V = \begin{pmatrix} \frac{1+\sqrt{2}}{\sqrt{4+2\sqrt{2}}} & 0 & \frac{1-\sqrt{2}}{\sqrt{4-2\sqrt{2}}} & 0\\ 0 & \frac{1+\sqrt{2}}{\sqrt{4+2\sqrt{2}}} & 0 & \frac{1-\sqrt{2}}{\sqrt{4-2\sqrt{2}}}\\ 0 & \frac{1}{\sqrt{4+2\sqrt{2}}} & 0 & \frac{1}{\sqrt{4-2\sqrt{2}}}\\ \frac{1}{\sqrt{4+2\sqrt{2}}} & 0 & \frac{1}{\sqrt{4-2\sqrt{2}}} & 0 \end{pmatrix}$$

$$(12)$$

as

$$V^{\dagger}U^{\dagger}hUV = t \times \text{Diag}\left(1 - \frac{\sqrt{2}}{2}, -1 + \frac{\sqrt{2}}{2}, 1 + \frac{\sqrt{2}}{2}, -1 - \frac{\sqrt{2}}{2}\right)$$
(13)

We therefore have the two lowest excited states with eigenenergies  $\pm t(1-\frac{\sqrt{2}}{2})$ 

$$\psi_{+1} = \Gamma U \begin{pmatrix} \frac{1+\sqrt{2}}{\sqrt{4+2\sqrt{2}}} \\ 0 \\ 0 \\ \frac{1}{\sqrt{4+2\sqrt{2}}} \end{pmatrix} = \Gamma \times \frac{1}{4\sqrt{2+\sqrt{2}}} \begin{pmatrix} 1+\sqrt{2}-\sqrt{3}i \\ (1+\sqrt{2})i-\sqrt{3} \\ i+\sqrt{3}+\sqrt{6} \\ 1+(\sqrt{3}+\sqrt{6})i \end{pmatrix}$$
(14)

$$\psi_{-1} = \Gamma U \begin{pmatrix} 0 \\ \frac{1+\sqrt{2}}{\sqrt{4+2\sqrt{2}}} \\ \frac{1}{\sqrt{4+2\sqrt{2}}} \\ 0 \end{pmatrix} = \Gamma \times \frac{1}{4\sqrt{2+\sqrt{2}}} \begin{pmatrix} (1+\sqrt{2})i - \sqrt{3} \\ 1+\sqrt{2}-\sqrt{3}i \\ 1+(\sqrt{3}+\sqrt{6})i \\ i+\sqrt{3}+\sqrt{6} \end{pmatrix}$$

The first excited states can therefore be understood as a hybridization between the "bulk" states of the 1-2 bond and the fermion on site 3. The other two eigenstates can be obtained similarly.

We next prove that in the braiding process given in the main text there is always a pair of MZM at exactly zero energy. Without loss of generality we consider the  $\phi_1 \to \phi_2$  step. The Hamiltonian in the fermion basis becomes

$$H = -e^{ix}c_{1}^{\dagger}c_{2} + c_{1}c_{2} + e^{-ix}c_{1}c_{2}^{\dagger} - c_{1}^{\dagger}c_{2}^{\dagger}$$

$$-e^{-\frac{\pi}{3}i}c_{2}^{\dagger}c_{3} + e^{\frac{2\pi}{3}i}c_{2}c_{3} + e^{\frac{\pi}{3}i}c_{2}c_{3}^{\dagger} - e^{-\frac{2\pi}{3}i}c_{2}^{\dagger}c_{3}^{\dagger}$$

$$+e^{\left(-\frac{\pi}{3}-x\right)i}c_{1}c_{3}^{\dagger} - e^{-\frac{2\pi}{3}i}c_{1}c_{3} - e^{\left(\frac{\pi}{3}+x\right)i}c_{1}^{\dagger}c_{3} + e^{\frac{2\pi}{3}i}c_{1}^{\dagger}c_{3}^{\dagger}$$

$$(15)$$

where we have temporarily omitted the energy unit t. We then have

$$[c_{1}^{\dagger}, H] = c_{2} + e^{-ix}c_{2}^{\dagger} + e^{\left(-\frac{\pi}{3} - x\right)i}c_{3}^{\dagger} - e^{-\frac{2\pi}{3}i}c_{3}$$

$$[c_{1}, H] = -[c_{1}^{\dagger}, H]^{\dagger} = -e^{ix}\left[c_{2} + e^{-ix}c_{2}^{\dagger} - e^{-\frac{2\pi}{3}i}c_{3} + e^{\left(-\frac{\pi}{3} - x\right)i}c_{3}^{\dagger}\right]$$

$$(16)$$

Therefore

$$\left[e^{\frac{ix}{2}}c_{1}^{\dagger} + e^{-\frac{ix}{2}}c_{1}, H\right] = 0 \tag{17}$$

Namely we have an MZM:

$$\tilde{a}_1 \equiv e^{\frac{ix}{2}} c_1^{\dagger} + e^{-\frac{ix}{2}} c_1 = C_{\frac{x}{2}} a_1 + S_{\frac{x}{2}} b_1 \tag{18}$$

To find the other MZM, we calculate the commutators between the other fermion operators with the Hamiltonian:

$$[c_{2}^{\dagger}, H] = e^{ix}c_{1}^{\dagger} - c_{1} - e^{-\frac{i\pi}{3}}c_{3} + e^{\frac{i\pi}{3}}c_{3}^{\dagger}$$

$$[c_{2}, H] = -e^{-ix}c_{1} + c_{1}^{\dagger} + e^{\frac{i\pi}{3}}c_{3}^{\dagger} - e^{-\frac{i\pi}{3}}c_{3}$$

$$[c_{3}^{\dagger}, H] = e^{-\frac{i\pi}{3}}c_{2}^{\dagger} + e^{-\frac{i\pi}{3}}c_{2} - e^{\frac{i\pi}{3}}c_{1} + e^{i(\frac{\pi}{3} + x)}c_{1}^{\dagger}$$

$$[c_{3}, H] = -e^{\frac{i\pi}{3}}c_{2} - e^{\frac{i\pi}{3}}c_{2}^{\dagger} + e^{-\frac{i\pi}{3}}c_{1}^{\dagger} - e^{-i(\frac{\pi}{3} + x)}c_{1}$$

$$(19)$$

Therefore

$$[c_2 - c_2^{\dagger}, H] = (1 - e^{-ix})c_1 + (1 - e^{ix})c_1^{\dagger}$$

$$[\left(e^{\frac{i\pi}{6}}c_3 - e^{-i\frac{\pi}{6}}c_3^{\dagger}\right), H] = e^{\frac{i\pi}{6}}(1 - e^{-i\left(\frac{\pi}{3} + x\right)})c_1 + e^{-\frac{i\pi}{6}}(1 - e^{i\left(\frac{\pi}{3} + x\right)})c_1^{\dagger}$$

$$(20)$$

However, the ratio between the coefficients of  $c_1$  or  $c_1^{\dagger}$  in the two commutators above is purely real:

$$-\frac{1 - e^{-ix}}{e^{\frac{i\pi}{6}}(1 - e^{-i(\frac{\pi}{3} + x)})} = -\frac{2 - 2\cos x}{e^{\frac{i\pi}{6}}(1 - e^{-i(\frac{\pi}{3} + x)})(1 - e^{ix})} = \frac{1 - \cos x}{\cos\left(x + \frac{\pi}{6}\right) - \frac{\sqrt{3}}{2}}$$
(21)

Thus the following Majorana operator commutes with the Hamiltonian and is the second MZM:

$$\tilde{b}_{23} \equiv -iN\left(\left[\cos\left(x + \frac{\pi}{6}\right) - \frac{\sqrt{3}}{2}\right]\left(c_2 - c_2^{\dagger}\right) + (1 - \cos x)\left(e^{\frac{i\pi}{6}}c_3 - e^{-\frac{i\pi}{6}}c_3^{\dagger}\right)\right) \\
= N\left(\left[\cos\left(x + \frac{\pi}{6}\right) - \frac{\sqrt{3}}{2}\right]b_2 + (1 - \cos x)\left(\frac{1}{2}a_3 + \frac{\sqrt{3}}{2}b_3\right)\right) \tag{22}$$

where N is a normalization factor. When x = 0 only the first term survives since

$$\lim_{x \to 0} \frac{1 - \cos x}{\cos \left(x + \frac{\pi}{6}\right) - \frac{\sqrt{3}}{2}} = 0 \tag{23}$$

while when  $x = -\frac{\pi}{3}$  only the second term survives. So  $\tilde{b}_{23}$  continuously evolves from  $b_2$  to  $\frac{1}{2}a_3 + \frac{\sqrt{3}}{2}b_3$  along the path  $\phi_1 \to \phi_2$ .

### II. MANY-BODY BERRY PHASE CALCULATION FOR THE 3-SITE KITAEV TRIANGLE

In this section we provide details for calculating the many-body Berry phase for braiding two MZM in the Kitaev triangle, as shown in Fig. 2 in the main text. To start we use the Hamiltonian Eq. (1) in the main text,

$$\mathcal{H} = \sum_{\langle jl \rangle} (-te^{i\phi_{jl}} c_j^{\dagger} c_l + \Delta e^{i\theta_{jl}} c_j c_l + \text{h.c.}) - \sum_j \mu c_j^{\dagger} c_j, \tag{24}$$

and write the creation and annihilation operators in the following Fock space basis for three spinless fermions

$$(|0\rangle, |1\rangle, \dots, |7\rangle) \equiv \{|n_1, n_2, n_3\rangle\}$$

$$= (|0, 0, 0\rangle, |0, 1, 0\rangle, |0, 0, 1\rangle, |0, 1, 1\rangle, |1, 1, 0\rangle, |1, 1, 1\rangle, |1, 1, 1\rangle, |1, 1, 1\rangle)$$

The creation(annihilation) operators in this space are defined as

$$c_j^{\dagger}|n_1,\dots,n_j,\dots\rangle = \sqrt{n_j+1}(-1)^{s_j}|n_1,\dots,n_j+1,\dots\rangle,$$

$$c_j|n_1,\dots,n_j,\dots\rangle = \sqrt{n_j}(-1)^{s_j}|n_1,\dots,n_j-1,\dots\rangle,$$
(25)

where

$$s_j = \begin{cases} \sum_{l=1}^{j-1} n_l & j > 1\\ 0 & j = 1 \end{cases}$$
 (26)

For the initial configuration corresponding to  $\phi_1$  in Eq. (6) of the main text, diagonalizing the  $8\times8$  BdG Hamiltonian in the above basis leads to two degenerate ground states that can be distinguished by the occupation number of the following fermion operator constructed from the two MZM at the two bottom vertices

$$c_M \equiv \frac{1}{2}(a_1 + ib_2), \ n_M \equiv c_M^{\dagger} c_M$$
 (27)

The two degenerate ground states for the initial configuration, denoted as  $|0\rangle_i$  and  $|1\rangle_i$ , therefore satisfy

$$n_M|0\rangle_i = 0,$$
 (28)  
 $n_M|1\rangle_i = |1\rangle_i$ 

In practice, we first construct the operator  $R_{\rm gs}$  as a  $8 \times 2$  matrix by combining the two column eigenvectors of the two lowest-energy eigenstates of the initial BdG Hamiltonian:

$$R_{\rm gs} \equiv (\psi_i, \psi_i') \tag{29}$$

and then diagonalize the projected  $n_M$  operator:

$$U_n^{\dagger}(R_{\rm gs}^{\dagger}n_M R_{\rm gs})U_n \equiv R_i^{\dagger}n_M R_i = \begin{pmatrix} 0 \\ 1 \end{pmatrix}$$
(30)

To carry out the Berry phase calculation we next need to adiabatically "rotate" the vector potential field by following the linearly interpolated closed parameter path described in the main text, which is discretized into N+1 segments. At any given point labeled by j along the path, we diagonalize the corresponding Hamiltonian and construct the projection operator  $P_j$  using the two lowest-energy eigenvectors  $\psi_j, \psi'_j$ :

$$P_j \equiv \psi_j \otimes \psi_j^{\dagger} + \psi_j' \otimes \psi_j'^{\dagger} \tag{31}$$

where  $\otimes$  means tensor product. The  $2 \times 2$  Berry phase matrix  $M_{f \leftarrow i}$  for the given parameter path is then obtained as

$$M_{f \leftarrow i} = \lim_{N \to \infty} R_f^{\dagger} P_N P_{N-1} \dots P_1 R_i \tag{32}$$

where  $R_f = R_i$  since the path is closed.

By using a large enough N we found the converged  $M_{f\leftarrow i}$  matrix has only diagonal elements being nonzero, meaning the braiding only changes each ground state by a scalar phase factor. Their values are  $(M_{f\leftarrow i})_{00} = e^{i0.118\pi}$  and  $(M_{f\leftarrow i})_{11} = e^{-i0.382\pi} = e^{i(0.118-0.5)\pi}$ .

We end this section by noting that the parameter path considered for the 3-site Kitaev triangle above is not equivalent to rotating a staggered vector potential but to separately manipulating the Peierls phases along the three edges. We have also done calculations for the latter case and found the two lowest-energy states fail to be degenerate everywhere along the parameter path, leading to non-standard relative Berry phases between the two initial states.

#### III. CORNER MZM IN FINITE-WIDTH HOLLOW TRIANGLES

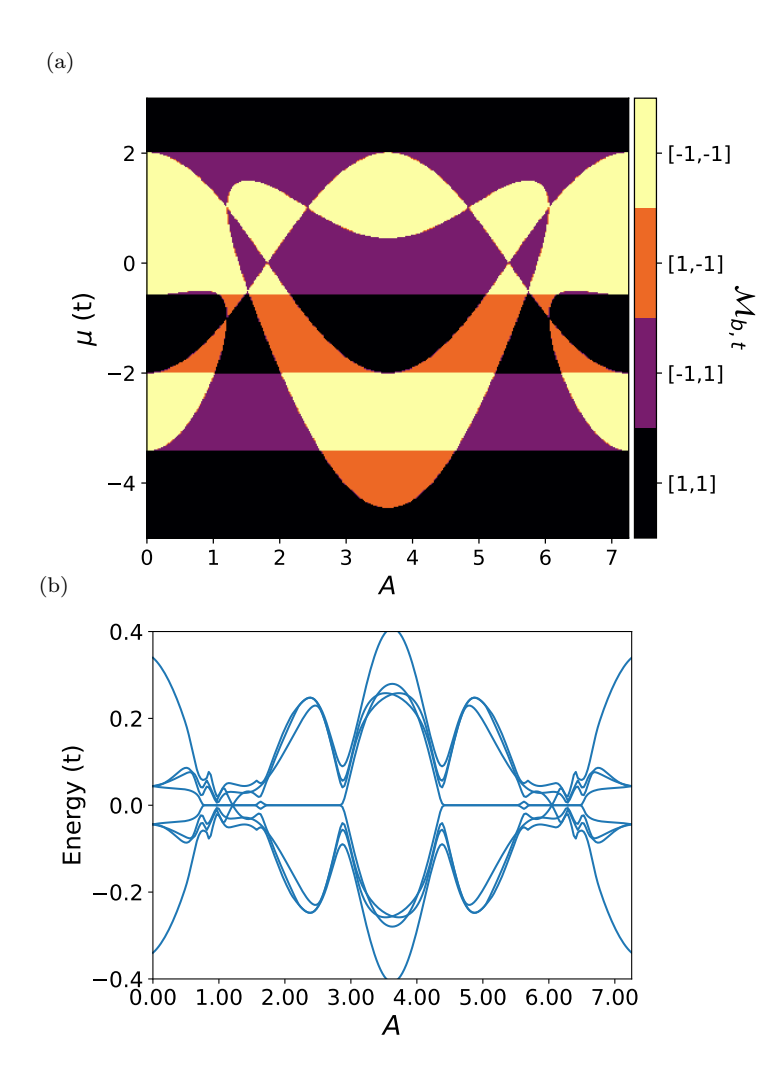


FIG. 1. (a) Topological phase diagram for a W=3 hollow triangle obtained by overlapping the  $\mathcal{M}_{b,t}(A,\mu)$  plots of 1D chains with  $\mathbf{A}=A\hat{\mathbf{y}}$  and  $\mathbf{A}=A(\frac{\sqrt{3}}{2}\hat{\mathbf{x}}+\frac{1}{2}\hat{\mathbf{y}})$ . Color scheme: purple— $[\mathcal{M}_b,\mathcal{M}_t]=[1,1]$ , yellow— $[\mathcal{M}_b,\mathcal{M}_t]=[-1,-1]$ , red— $[\mathcal{M}_b,\mathcal{M}_t]=[-1,1]$ , orange— $[\mathcal{M}_b,\mathcal{M}_t]=[1,-1]$  (b) Near-gap BdG eigen-energies vs A for a finite triangle with edge length L=80, W=3, and  $\mu=1.6$ .

A model that is closer to a realistic hollow triangular island is the finite-width triangular chain or ribbon. An example, illustrated in Figure 2 (d), has its edge length L=80 and width W=3. The Hamiltonian for a single ribbon parallel to  $\hat{\mathbf{x}}$  is constructed and Fourier transformed in the way described in the main text and has the following block form up to a constant

$$\mathcal{H} = \frac{1}{2} \sum_{k} \Psi_{k}^{\dagger} \begin{pmatrix} h_{t}(k) & h_{\Delta}(k) \\ h_{\Delta}^{\dagger}(k) & -h_{t}^{*}(-k) \end{pmatrix} \Psi_{k}$$
(33)

where  $\Psi_k \equiv (c_{k,1}, \dots, c_{k,W}, c_{-k,1}^{\dagger}, \dots c_{-k,W}^{\dagger})^T$ .  $h_t(k)$  is a  $W \times W$  Hermitian tridiagonal matrix with  $(h_t)_{n,n} = -2t\cos(k + \mathbf{A} \cdot \mathbf{a}_1) - \mu$  and  $(h_t)_{n,n+1} = -t\left(e^{i(-k + \mathbf{A} \cdot \mathbf{a}_3)} + e^{i\mathbf{A} \cdot \mathbf{a}_2}\right)$  (here  $\mathbf{a}_3 \equiv -\mathbf{a}_1 + \mathbf{a}_2$ ).  $h_{\Delta}(k)$  is a  $W \times W$  tridiagonal matrix with  $(h_{\Delta})_{n,n} = -2i\Delta \sin k$  and  $(h_{\Delta})_{n,n\pm 1} = \mp \Delta \left[e^{-i(\pm k + \frac{2\pi}{3})} + e^{-i\frac{\pi}{3}}\right]$ .

The phase diagram Fig. 1 (a) is created in a similar way as that in Fig. 3 (b) of the main text, assuming a constant vector potential along  $\hat{\mathbf{y}}$  and infinitely long W=3 ribbons. The spectral flow for the actual triangle with  $\mu=1.6$  in Fig. 1 (b) shows MZM in the parameter regions in agreement with the phase diagram. Fig. 1. The MZM wavefunctions for A=0.83 and  $\mu=1.6$ , illustrated in Fig. 2 (d), are indeed well localized at the bottom corners.

We next discuss how to move the MZM on a hollow triangle by rotating the vector potential. Due to the Peierls phase accumulated by hopping that is not parallel with the finite-width ribbon edges, the vector potential has a more complex effect on the energy spectrum here than that for the W=1 case. To ensure that the bulk band gap of individual edges only closes at a few isolated topological phase transition points, we plot in Figure 2 (b) the smallest gap of the three edges with periodic boundary condition versus  $(A, \varphi)$  when  $\mu = 1.6$ . A relatively clean region can be identified when  $A \in (0.75, 0.8)$ . Further taking into account the topological phase diagram Fig. 2 (a) obtained in a similar way as Fig. 4 (a) in the main text, we chose a parameter path on the  $(A, \varphi)$  plane that linearly interpolates the following points:

$$(A,\varphi) = (0.83,0) \to \left(0.77, \frac{\pi}{6}\right) \to \left(0.83, \frac{\pi}{3}\right) \to \left(0.77, \frac{\pi}{2}\right)$$
 (34)

The phase diagram indicates that along this path, the nontrivial  $\mathcal{M} = -1$  phase crawls through the three edges in a clockwise manner. Such a path ensures that only one edge undergoes a topological phase transition at a time. Then in the actual triangle the bulk gap will stay open due to finite size effect as a MZM moves across an edge without hybridizing with the other MZM.

To support this claim, we plot in Fig. 2 (c) the spectral flow for a finite triangle with L=80, W=3,  $\mu=1.6$  and the above parameter path. The bulk gap is indeed open throughout the path, and the degeneracy of the two MZM also stays intact. The wavefunctions of the MZM at representative points along the path are plotted in panels (d-g) in the same order as that marked in panel (c). The locations of the MZM are also consistent with that inferred from the topological phase diagram.

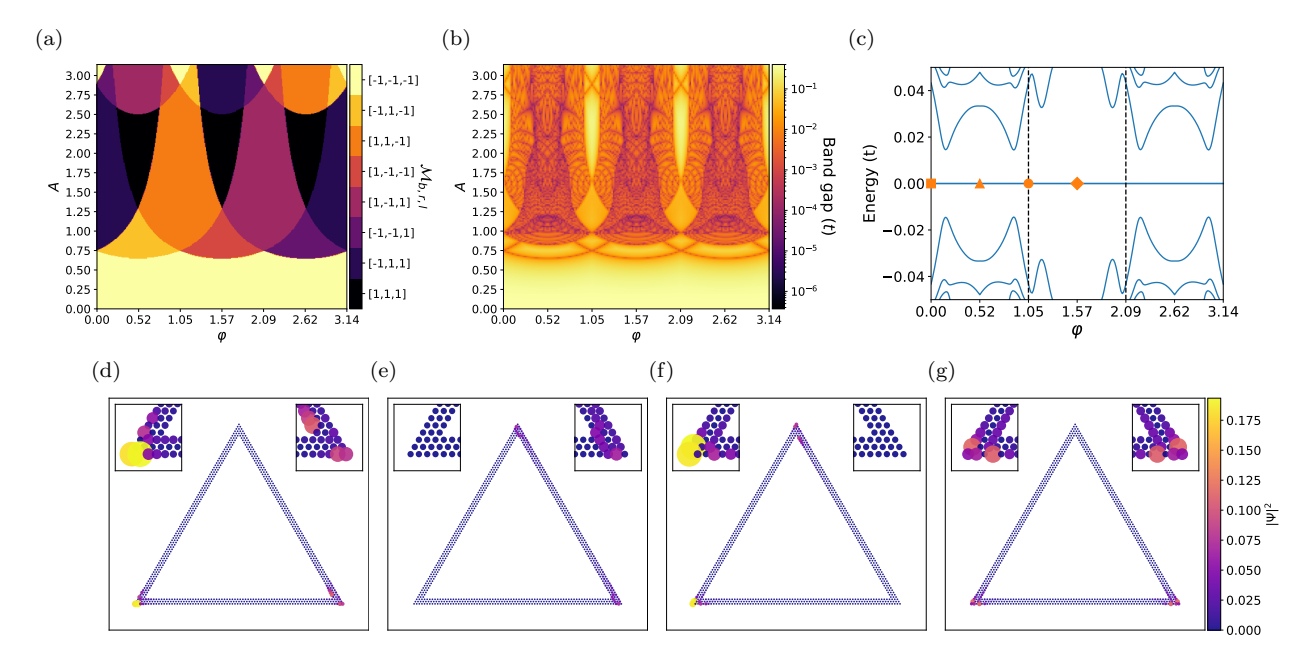


FIG. 2. (a) Topological phase diagram for three W=3 ribbons corresponding to the three edges of a hollow triangle. ( $\mu=1.6$  in all panels.) (b) Minimum of the bulk gaps of the three ribbons plotted on the  $(A,\varphi)$  plane. (c) Spectral flow of a hollow triangle with W=3, L=80, and the parameter path given in Eq. (34). (d-g) BdG eigenfunction  $|\Psi|^2$  summed over the two zero modes at  $\varphi=0,\frac{\pi}{6},\frac{\pi}{3},\frac{\pi}{2}$ , respectively.

## IV. BRAIDING MZM IN A SMALL NETWORK OF TRIANGLES

In this section we show that one can braid two out of four MZM, a minimal setting for nontrivial manipulation of the degenerate many-body ground states, by using a small network of corner-sharing triangles. We focus on the critical step of swapping  $\gamma_2$  and  $\gamma_3$  as labeled in Fig. 5 of the main text. This can be done by rotating the vector potential of the triangle in the middle of the bottom row from  $\varphi = \frac{\pi}{6}$  to  $\frac{\pi}{3}$ . More specifically, when  $\varphi = \frac{\pi}{6}$ , with the chosen values of  $\mu$  and A, only the right edge of the said triangle is topologically nontrivial. The chain that hosts  $\gamma_{3,4}$  thus extends through this nontrivial edge to the top triangle as in Fig. 3 (b). On the other hand, when  $\varphi$  increases to  $\frac{\pi}{3}$ , the nontrivial edge of the middle triangle changes from right to left, which leads to  $\gamma_2$  hopping from its left

corner to the right through the top corner, while  $\gamma_3$  is unaffected [Figs. 3 (c-g)]. As a result the  $\gamma_2, \gamma_3$  swapping is done without closing the bulk gap, as can be seen from the spectral flow in Fig. 3 (a).

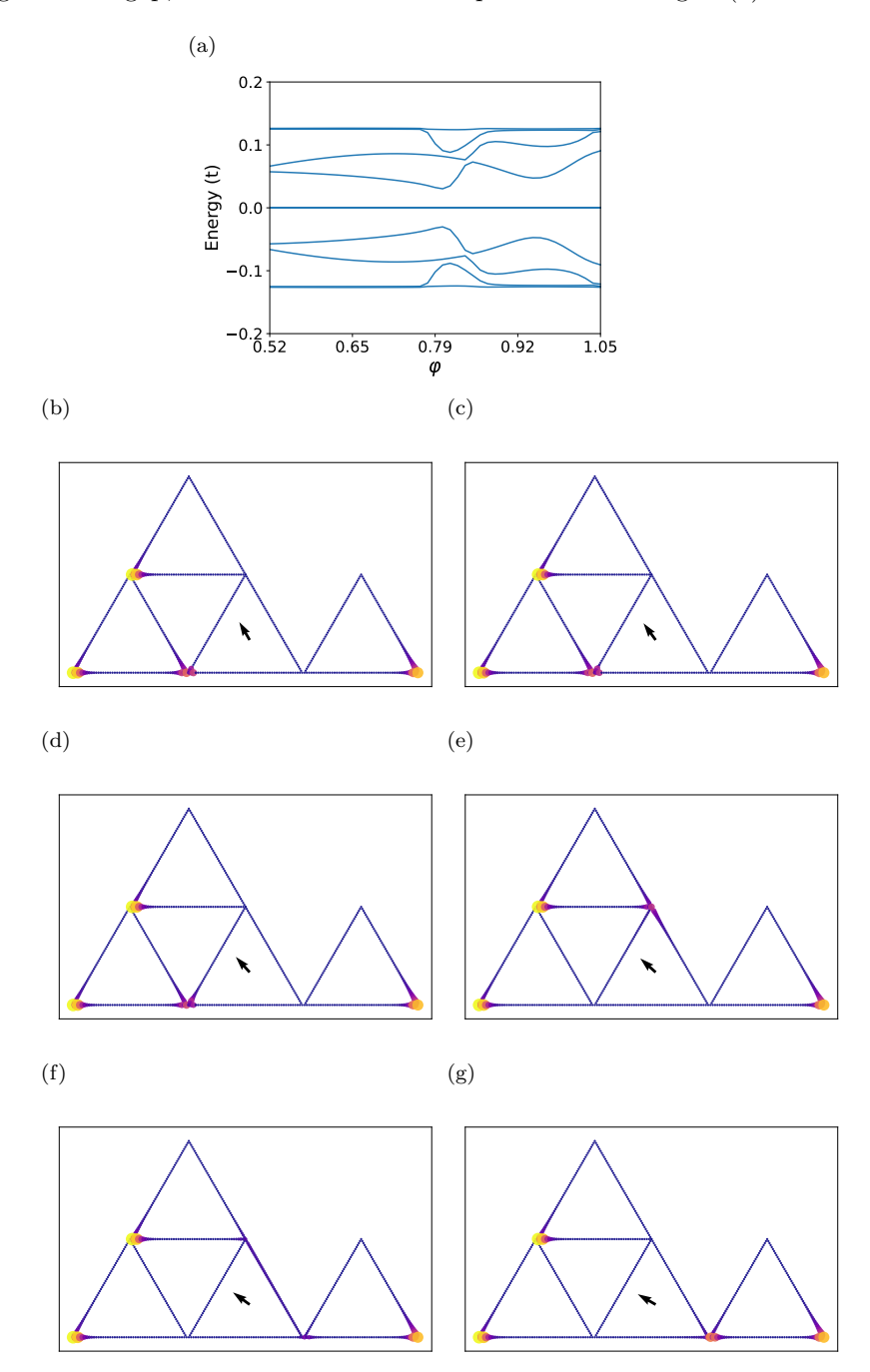


FIG. 3. (a) Spectral flow for the critical step of swapping  $\gamma_2$  and  $\gamma_3$  in the example of Fig. 5 in the main text, calculated using four corner-sharing triangles of W=1 and L=50, with  $\mu=1.6$  and A=2.6. Vector potential for the middle triangle in the bottom row can rotate according to  $\mathbf{A}=A(-\sin\varphi\hat{\mathbf{x}}+\cos\varphi\hat{\mathbf{y}})$  from  $\varphi=\frac{\pi}{6}$  to  $\frac{\pi}{3}$ , while the other three have fixed  $\varphi=0$ . (b)-(g) BdG eigenfunction  $|\Psi|^2$  summed over the four zero modes at equally-spaced points along the rotation path. The black arrow indicates the direction of the vector potential for the bottom middle triangle.